RESEARCH ARTICLE OPEN ACCESS

Dihydroartemisinin Attenuates Radiation-Induced Lung Injury by Inhibiting the cGAS/STING/NF-κB Signaling Pathway

Cailan Wang | Xinyi Lin | Shichun Guan | Qiaoyuan Wu | Shixiong Liang [iD]

Department of Radiation Oncology, Guangxi Medical University Cancer Hospital, Nanning, China

Correspondence: Qiaoyuan Wu (1258838303@qq.com) | Shixiong Liang (liangshixionglsx@163.com)

ABSTRACT

Dihydroartemisinin (DHA) is a derivative of artemisinin, which affects inflammation, oxidative stress, and immune regulation. However, the mechanism underlying its effects remains largely unknown. This study aims to explore the mechanism by which DHA affects radiation-induced lung injury (RILI), providing new insights for lung radiotherapy. To elucidate its mechanism of action, C57BL/6 J mice were irradiated with 15 Gy whole chest. RILI was evaluated by qRT-PCR, ELISA, histology, Western blot analysis, immunohistochemistry, and RILI signaling cascade studies. In addition, small interfering RNAs were employed to knockdown cGAS proteins in the cGAS-STING signaling pathway in the human bronchial epithelium cell line (BEAS-2B). Both In Vivo and Vitro experiments were conducted to investigate the specific mechanism by which DHA alleviated RILI. We observed the activation of the cGAS-STING pathway, along with the phosphorylation of the downstream target NF-κB and an increase in inflammatory factor levels in the mouse model following radiation exposure. In the cell model, irradiation also triggered the activation of the cGAS-STING signaling pathway and its downstream targets, leading to elevated levels of inflammatory factors. Notably, knocking down the cGAS using small interfering RNA in the BEAS-2B cells significantly alleviated RILI in the cell model. Our study elucidated the mechanism of DHA reducing RILI through the cGAS/STING/NF-κB signaling pathway, and revealed that the GAS/STING/NF-κB axis may be a potential therapeutic target for RILI.

1 | Introduction

Radiotherapy (RT) is one of the primary treatment options for thoracic cancers. However, the lung is the primary dose-limiting organ in the thorax because it is an organ that is susceptible to ionizing radiation (Hanania et al. 2019). Patients' quality of life is impacted by radiation-induced lung damage (RILI), which causes early and late molecular and cellular toxicities, some of which are irreversible (Curras-Alonso et al. 2023).

Direct DNA damage and the production of reactive oxygen species are the primary processes that cause RILI. These events trigger intracellular signaling and lead to the release of various molecules and cytokines to promote inflammation and the immune response (Abratt et al. 2004; Azzam et al. 2012). After irradiation, cells generate DAMP molecules, which aid in attracting neutrophils, macrophages, leukocytes, and lymphocytes (Ryter et al. 2007). Many cytokines, including interleukin 3 (IL-3), interleukin 6 (IL-6), interferon-γ, transforming growth

---

factor β (TGF-β), tumor necrosis factor α (TNF-α), and HMGB1, build up in damaged lung tissue as a result of immune cell transmigration. Through a variety of signaling pathways, these occurrences trigger an inflammatory response that results in acute pneumonitis and persistent lung fibrosis (Barker et al. 2015). The three primary signaling pathways of RILI include TGF-β/SMAD signaling pathway, HMGB1/TLR4 signaling pathway and Nrf2/ARE signaling pathway (Ning et al. 2024).

Additionally, damage-associated signaling pathways, such as ROS/reactive nitrogen species and cGAS-STING, contribute to the initial process of lung injury, with activated cGAS triggering innate immunity by releasing cyclic GMP-AMP (cGAMP), which binds to and activates STING (Benmerzoug et al. 2018; Chen et al. 2016). The primary regulator of the inflammatory response, NF-κB, has been linked to the synthesis of numerous inflammatory cytokines and chemokines, including TNF-α, IL-1β, and IL-6 (Zhong et al. 2024). The pathophysiology of RILI is mostly mediated by these cytokines (Carvalho et al. 2019). Nevertheless, little is known about the underlying processes of pulmonary inflammation on aberrant dsDNA sensing via the cGAS-STING pathway after thoracic RT.

Artemisinin is derived from the annual herb *Artemisia annua* L., which has been used as traditional medicine for over 2000 years. Dihydroartemisinin (DHA) is the first-generation derivative of this compound. Artemisinin and its derivatives (ARTs) have cured over one million malaria patients (Dai et al. 2021). The molecular formula of DHA is $C_{15}H_{24}O_5$ and the molecular weight is 284.35 (Figure S1. Images from PubChem database). Artemisinin traditionally used to treat malaria, recent studies have discovered that its derivatives also exhibit anti-inflammatory, anti-fibrotic, and immunoregulatory effects (Li et al. 2006; Xu et al. 2007), and some studies have shown that it plays an important role in oxidant stress in cancer pathogenesis (Dai et al. 2021). In our previous study, DHA treatment was found to attenuate RILI in mice (Ning et al. 2024). These indicated that DHA has some protective effects in RILI. However, the specific role in RILI remains not well understood. To address this, our study investigated whether the protective effects of DHA were linked to the activation of the cGAS/STING/NF-κB pathway and whether DHA can mitigate RILI by inhibiting this pathway. We assessed the protective effects of DHA on RILI by exposing BEAS-2B cells and C57BL/6 mouse to DHA along with the indicated radiation dose. This study aims to establish a solid theoretical foundation for the prevention and treatment of RILI.

2 | Materials and Methods

2.1 | Animals

Male C57BL/6 mice (6–8 weeks old, 18–22 g) were provided by the Guangxi Medical University Animal Experiment Center, China. The mice were kept in a ventilated environment with ad libitum feeding and watering at a constant temperature of $24°C \pm 1°C$. The Guangxi Medical University Institutional Ethics Committee gave its approval to the study (No. KY-2023-505).

2.2 | Animal Irradiation

The modeling of RILI was informed by existing literature on RILI mouse models and pre-validated basic research on successful models (Ning et al. 2024; Wang et al. 2023). The mice were anesthetized by intraperitoneal injection of 1% sodium pentobarbital (50 mg/kg). Following anesthesia, mice were irradiated with a single vertical thoracic irradiation with X-rays from a 6 MV linear accelerator (Elekta, Versa HD, Sweden) at a single dose of 15 Gy (source to axis distance of 100 cm and dose rate of 600 MU/min).

2.3 | Drug Management

In the preliminary experiments of this study, we chose doses of 10, 50, 100, and 200 mg/kg/day to test the protective effect of DHA (71939-50-9, Aladdin, Shanghai, China, 98% purity) against RILI. The mice were gavaged with DHA once a day for 30 days starting on the second day of irradiation. Then, we divided the mice into simple dosing groups with different drug concentrations (10, 20, 50, and 100 mg/kg/day) without irradiation treatment, and gavaged DHA daily for 30 days. Lung tissue specimens were collected on the 30th day for HE staining. Based on the existing literature (Li, Sun, et al. 2019; Li, Zhou, et al. 2019) and our preliminary experimental results, the dose of 50 mg/kg/day was chosen in this study to test the protective effect of DHA against RILI. In this experiment, we randomly divided the mice into three groups: control group, irradiation group, irradiation + DHA group. In addition to the control group, two other groups of mice were also subjected to RILI modeling. Since the second day of irradiation, both control and irradiation groups were given placebo. The irradiation + DHA group received daily gastric gavage of DHA (50 mg/kg). The treatment was carried out for 30 consecutive days. The experimental plan is displayed in (Figure 1A).

2.4 | Mouse Tissue Samples

Tissue sampling was executed on Day 30 after irradiation. Blood was collected from the heart and allowed to sit at room temperature for 2 h before being centrifuged for 15 min (4°C, 665 RCF). The resulting serum was kept at −80°C in a freezer. Fresh lung tissue was taken from both sides, preserved at −80°C for WB analysis, and submerged in 4% (w/v) paraformaldehyde for immunohistochemistry (IHC), Masson's trichrome staining, and hematoxylin and eosin (H&E).

2.5 | Cell Culture and Knockdown of cGAS

Human bronchial epithelial cell line (BEAS-2B) cells were earned from Cell Bank of the Chinese Academy of Science. Cells were grown in DMEM medium (Gibco, New York, USA) containing 10% FBS in a 37°C, 5% CO_2 incubator. The cells were passaged three times a week as per established experimental protocols.

BEAS-2B cells were seeded in six-well plates and allowed to reach 70% confluence after 24 h. Cells were transfected with plasmids for si-cGAS, and negative controls (20 uM, Gene) using Lipofectamine 3000 reagent by following the user manual. Cells were harvested for RNA extraction and protein extraction 48 h after transfection, respectively. The following siRNAs were used:
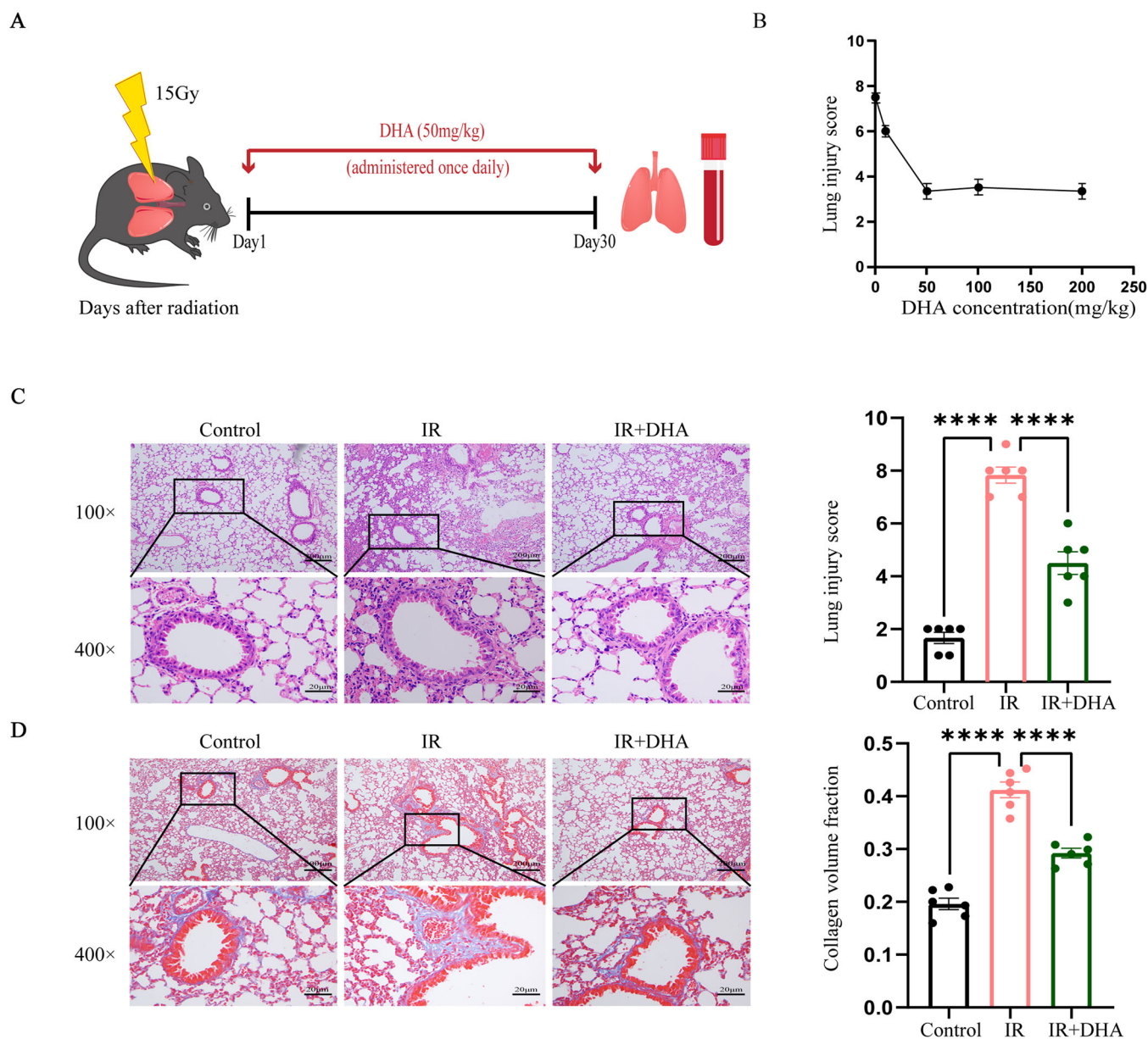
FIGURE 1 | DHA significantly alleviated radiation-induced lung injury in C57BL/6. (A) The scheme of DHA treatment study. (B) Dose-effect curves for DHA dose and HE pathology scores. (C) Representative H&E staining and the lung injury scores; scale: 200 μm (×100) and 20 μm (×400). (D) The representative Masson trichrome dyeing and the comparison of collagen volume fraction in each group; scale: 200 μm (×100) and 20 μm (×400). DHA, dihydroartemisinin; H&E, hematoxylin and eosin; IR, irradiation; IR + DHA, irradiation + DHA. $*p < 0.05$, $**p < 0.01$, $***p < 0.001$, $****p < 0.0001$.

cGAS-homo-774, 5′-GGAGCUACUAUGAGCACGUUTT-3′

cGAS-homo-1054, 5′-CCCUGCUGUAACACUUCUUTT-3′

cGAS-homo-1266, 5′-GGCUAUCCUUCUCUCACAUT-3′

cGAS-homo-1460, 5′-GCCUUCUUUCACGUAUGUATT-3′

2.6 | RNA-Seq

C57BL/6 mice samples were used to RNA-Seq analysis by Majorbio (Shanghai, China). In short, following ribosomal RNA depletion, mRNA, lncRNA, and circRNA libraries were created using the Total RNA-seq (H/M/R) Library Prep Kit (Illumina).

Following the completion of RNA library creation and quality testing using an Agilent 2100 Bioanalyzer, high throughput sequencing was carried out to retrieve raw reads on an Illumina HiSeq X10 PE150 (Illumina, San Diego, CA). Following the removal of low-quality data, jointed-sequence reads, and reads with many N sequences from raw reads, clean reads were chosen. Additionally, effective readings were obtained after ribosomal RNA sequences were removed. After eliminating low-quality and linker-containing sequences from the original sequence data, we were left with clean reads. The NCBI database provided the reference genomes, which were then aligned using the Tophat program. Genes with differential expression were screened using the DESeq. 2 R program, and genes with differential expression were characterized as FDR < 0.05 and FC > 2. The clusterProfiler tool for KEGG (Kyoto encyclopedia

of genes and genomes) enrichment analysis was also used in the study. The analysis parameter setting adopts the software default setting, the network specificity option is medium, and the result is shown when $p < 0.05$.

2.7 | Lung Histology and IHC

Following normal protocols, the lung tissues were fixed in 4% (w/v) paraformaldehyde solution, embedded in paraffin, sliced at 5 μm, and stained with Masson trichrome and H&E. For IHC, the paraffin sections were incubated overnight at 4°C with primary antibodies against cGAS (1:1000, Cell Signaling Technology), STING (1:1000, Cell Signaling Technology), TGF-β (1:100, Servicebio), IL-6 (1:500, Servicebio) and TNF-α (1:500, Servicebio), succeeded by incubation at 37°C for 60 min with mouse secondary antibody (1:200; Servicebio). The Szapiel scoring method was used to assess the severity of pulmonary fibrosis sores and alveolitis. The optical density was assessed using Image Pro Plus (Media Cybernetics). The Image Pro Plus was used for semi-quantitative analysis of cGAS, STING, TNF-α, TGF-β, and IL-6 and the collagen volume fraction (CVF) for each field was calculated as follows: CVF = collagen area in the field/total field area ×100.

2.8 | Western blot

The lung tissue or cells were added to protease inhibitors and RIPA lysate, and the tissue is then ground. The samples were fully lysed at 4°C for 30 min and centrifuged at 12,000g for 15 min. Following SDS-PAGE, 20 microgram aliquots of protein lysate were transferred onto 0.22 μm Polyvinylidene Difluoride Membrane and treated with primary antibodies; The followed rabbit-derived primary antibodies were used: β-actin (1:1000, Cell Signaling Technology), cGAS (1:1000, Cell Signaling Technology), STING (1:1000, Cell Signaling Technology), p65 (1:1000, Cell Signaling Technology), p-p65 (ser 536, 1:1000, Cell Signaling Technology). The membrane was then incubated with goat anti-rabbit IgG fluorescent secondary antibody (1:30,000, Cell Signaling Technology) at room temperature for 1 h. And imaging was performed using a fluorescent imager. The bands were examined and evaluated using Image J software (National Institutes of Health, Bethesda, Maryland, USA).

2.9 | Real-Time Quantitative Polymerase Chain Reaction (qPCR)

TRIzol reagent (Takara) was used to extract total RNA from cells in accordance with the manufacturer's instructions. cDNA was synthesized using the PrimeScriptTM FAST RT reagent Kit with gDNA Eraser (Takara Bio, Japan) and qPCR analysis was performed using TB green Premix Ex Taq Ⅱ (Tli RNaseH Plus) (Takara Bio, Japan) in the real-time detection system (qTOWER3G, Germany). The $2^{-\triangle\triangle C_t}$ technique was used to standardize the relative expression level of mRNA to that of endogenous control β-actin. The primer sequences indicated below were found in Table 1 and Table S3.

2.10 | Cell Viability Assay

The BEAS-2B cells were cultured in the 96-well plate, five repetitions of each. Each well received 100 μL of the Cell Counting Kit-8 (CCK-8) (Meilunbio, China) solution, which was then incubated for 2 h at 37°C. A multi-plate reader (infinite-M200, Austria) was used to measure the optical density value at 450 nm. Experiments were repeated three times.

2.11 | Enzyme-Linked Immunosorbent Assay (ELISA)

The levels of TGF-β1, IL-6, and TNF-α in cell supernatants, serum, or lung tissue homogenate were measured using an Elisa kit depending on the manufacturer's instructions (Elabscience, Wuhan, China).

2.12 | Molecular Docking

Autodock simulation using Autodock 4.2 software. First, the cGAS protein (Uniprot ID: Q8C6L5) was downloaded from the Uniprot database. The three-dimensional structure of small molecule DHA was obtained from PubChem database (PubChem ID: 3000518). Then the protein was designated as the receptor, and the small molecule DHA was designated as the ligand. AutodockTools 1.5.6 software was used for hydrogenation, checking and calculating the charge and constructing the docking grid box of the protein structure. In addition, small molecule ligands select the reversible bond of the ligand in AutodockTools. Finally, both the protein structure and the small molecule ligand format should be converted to the PDBQT format using AutoDockTools software for further docking. After docking with Vina, the scores of proteins and small molecule docking combinations were calculated, and the force analysis and visualization of three-dimensional and two-dimensional angles were performed using PyMOL 2.5 and Discovery Studio software.

2.13 | Statistical Analysis

The means ± standard deviation were used to display all of the data. GraphPad Prism 9 (USA) was used to conduct the statistical analysis. An unpaired t-test was used for two-group comparisons. One-way analysis of variance was used to compare several groups. Nonparametric statistical analysis was used to examine these nonnormally distributed data. Every experiment was conducted three times on its own. $p < 0.05$ was accepted as statistically significant.

3 | Results

3.1 | DHA Alleviates RILI in C57BL/6

We used 15 Gy single whole-lung irradiation to establish a mouse RILI model. We then assessed lung injury based on pathologic scores reported at an American Thoracic Society

Symposium (Matute-Bello et al. 2011). In the preliminary experiments of this study, we constructed a RILI mouse model and administered different doses of DHA daily by oral gavage for 30 days. The dose-effect curves were then plotted according to the drug dose and HE pathology scores and the ID_{50}. The results showed that the HE score decreased with the increase of dose, indicating that DHA had a mitigating effect on radiological lung injury with an ID_{50} of about 10.72 mg/kg (Figure 1B). In addition, we further divided the mice into different drug concentration dosing groups without irradiation treatment. H&E staining revealed no pathological damage, such as inflammatory cell infiltration in all groups (Figure S2). In this experiment, HE results showed that the mice in the control group had normal alveolar structure, a distinct lung texture, and no visible signs of alveolar wall rupture or hemorrhage. Compared to the control group, mice in the irradiation group exhibited noticeably thicker alveolar septa, disordered alveolar architecture, and exudates in their alveoli. Numerous inflammatory cells were shown to be present in the alveolar cavity and interstitial space. Lung tissue damage and inflammatory cell infiltration were reduced in the irradiation + DHA group compared to the irradiation group (Figure 1C). The irradiation + DHA group's pathologic scores were lower than the irradiation group's, whereas the irradiation group's pathologic scores were significantly higher than the control group's (Figure 1C). Masson's trichrome staining was used to observe the collagen deposition of the lungs of mice. The results of Masson's trichrome staining shown that there was no obvious collagen fiber deposition in the control group, but obvious collagen deposition was visible in the irradiation group, and was significantly reduced in the DHA treatment group (Figure 1D). It can be revealed that DHA can alleviate some of the irradiation induced lung inflammation and lung fibrosis.

In addition, we detected the expression levels of TGF-β, IL-6, and TNF-α through IHC assay and ELISA assay. The IHC assay results demonstrated that TGF-β, IL-6, and TNF-α were mainly expressed in the bronchial epithelial cells, with a lower expression observed in the lung parenchyma. TGF-β, IL-6, and TNF-α levels were elevated in the irradiation group compared to the control group, but were decreased in the irradiation + DHA group compared to the irradiation group (Figure 2A,B). According to the ELISA assay results, the irradiation group had significantly higher levels of TGF-β, IL-6, and TNF-α than the control group. In contrast, the irradiation + DHA group had lower levels of these substances (Figure 2C), which was consistent with the IHC assay results. This suggested that DHA attenuated levels of TGF-β, IL-6, and TNF-α, thereby reducing lung damage.

3.2 | DHA Attenuates RILI by Inhibiting cGAS/STING/NF-κB Signaling

To further explore the specific mechanism of DHA attenuating RILI, we performed transcriptome sequencing on the tissues of the control group and the irradiation group, and found that STING was significantly different and enriched to the NF-κB pathway by KEGG (Figure 3A,B). In addition, excitingly, molecular docking analysis showed that DHA had a strong affinity with cGAS protein through hydrogen bonds (TYR, HIS),

suggesting that cGAS may be a key target for DHA as a selective treatment for RILI (Figure 3C). According to IHC data, the irradiation group had significantly higher levels of cGAS and STING expression, while the DHA treatment group had significantly lower levels than the irradiation group (Figure 3D). The WB results shown that, compared to the control group, the expression levels of cGAS, STING, and p-NF-κB were significantly increased in the irradiation group, while NF-κB levels did not show a significant change; in contrast, the expression levels of cGAS, STING, and p-NF-κB were significantly reduced in the DHA treatment group compared to the irradiation group (Figure 3E). In conclusion, our results indicated that DHA can inhibit the cGAS/STING/NF-κB signaling pathway, ultimately protecting mice from RILI.

3.3 | DHA can Reduce the Damage of BEAS-2B Cells

First, CCK8 analysis was performed to assess the toxic effects of different concentrations (0, 5, 15, 25, and 45 μM) of DHA on BEASB-2B cells. The IC_{50} values of DHA on BEASB-2B cells were 18.33, 12.06, and 11.91 μM after 24, 48, and 72 h, respectively (Figure 4A). We selected the radiation doses (0, 2, 4, 6, 8, and 10 Gy) at different time points (24, 48, and 72 h) in BEAS-2B cells to clarify its sensitivity to radiation. The CCK8 results indicated that when the radiation dose increased to 8 Gy, the cell viability decreases to 50% after 72 h, suggesting cellular damage (Figure 4B). Therefore, 8 Gy was subsequently chosen as the irradiation dose. In addition, to further screen for the optimal concentration that could protect BEASB-2B cells from radiation damage, we administered different concentrations of DHA (0, 3, 6, and 9 μM) to the cells before irradiation. The CCK8 results shown that cell viability was highest at a drug concentration of 6 μM after 48 h of irradiation compared to the control and IR groups (Figure 4C). Therefore, we selected 6 μM as the drug concentration for subsequent experiments.

To further verify the effect of DHA on RILI, we used qPCR assay to detect the gene expression levels of TGF-β, IL-6, and TNF-α in the BEAS-2B cells. The results shown that TGF-β, IL-6, and TNF-α gene expression levels were significantly increased in the irradiation group compared to the control group, while these levels decreased in the cells of DHA-treated cells compared to the irradiation group (Figure 4D). Additionally, we used ELISA assay to detect the levels of TGF-β, IL-6, and TNF-α in the culture medium of BEAS-2B cells. Further ELISA assay also shown that DHA reduced the levels of TGF-β, TNF-α, and IL-6 (Figure 4E). In summary, our results suggest that DHA can reduce the damage of radiation to cells.

3.4 | DHA Alleviates Radiation Damage to Cells by Inhibiting cGAS/STING/NF-κB Signaling Pathway

To show the effect of DHA on IR-induced activation of cGAS/STING/NF-κB pathway, BEAS-2B cells pretreated with 6 μM DHA for 2 h were then exposed to 8 Gy irradiation for 48 h, and detected for the protein expression of cGAS, STING,
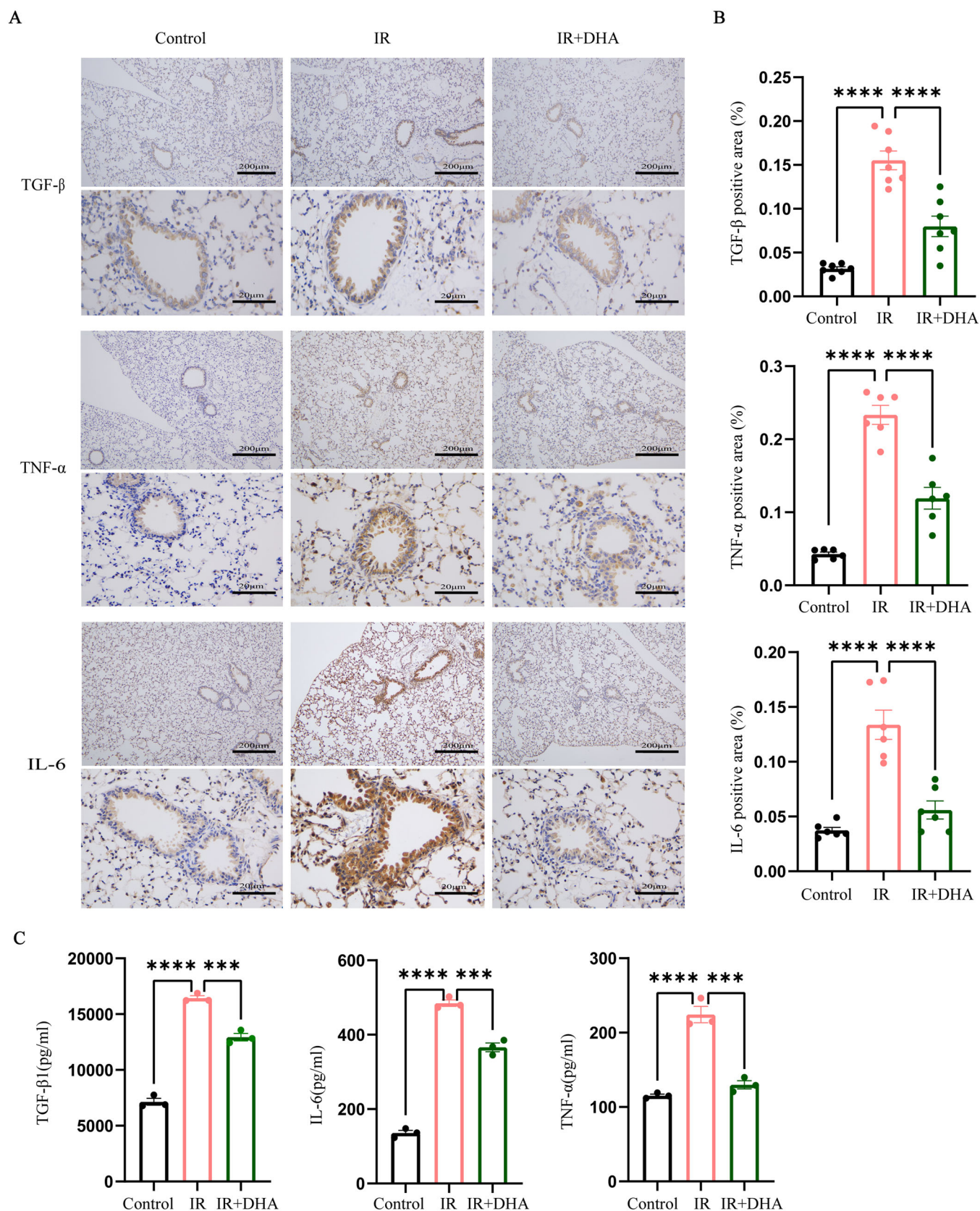
FIGURE 2 | DHA inhibited the expression of inflammatory factors in lung tissue of mice. (A) Representative TGF-β, IL-6, and TNF-α IHC staining and semi-quantitative analysis were performed in mouse lung tissues. scale: 200 μm (×100) and 20 μm (×400). (B) TGF-β-positive area ratios, TNF-α-positive area ratios and IL-6-positive area ratios. (C) The levels of TGF-β, IL-6, and TNF-α in serum and lung homogenate of mice were detected by ELISA. DHA, dihydroartemisinin; IHC, immunohistochemistry; IL-6, interleukin-6; IR, irradiation; TGF-β, transforming growth factor-β; TNF-α, tumor necrosis factorα. $*p < 0.05$, $**p < 0.01$, $***p < 0.001$, $****p < 0.0001$.
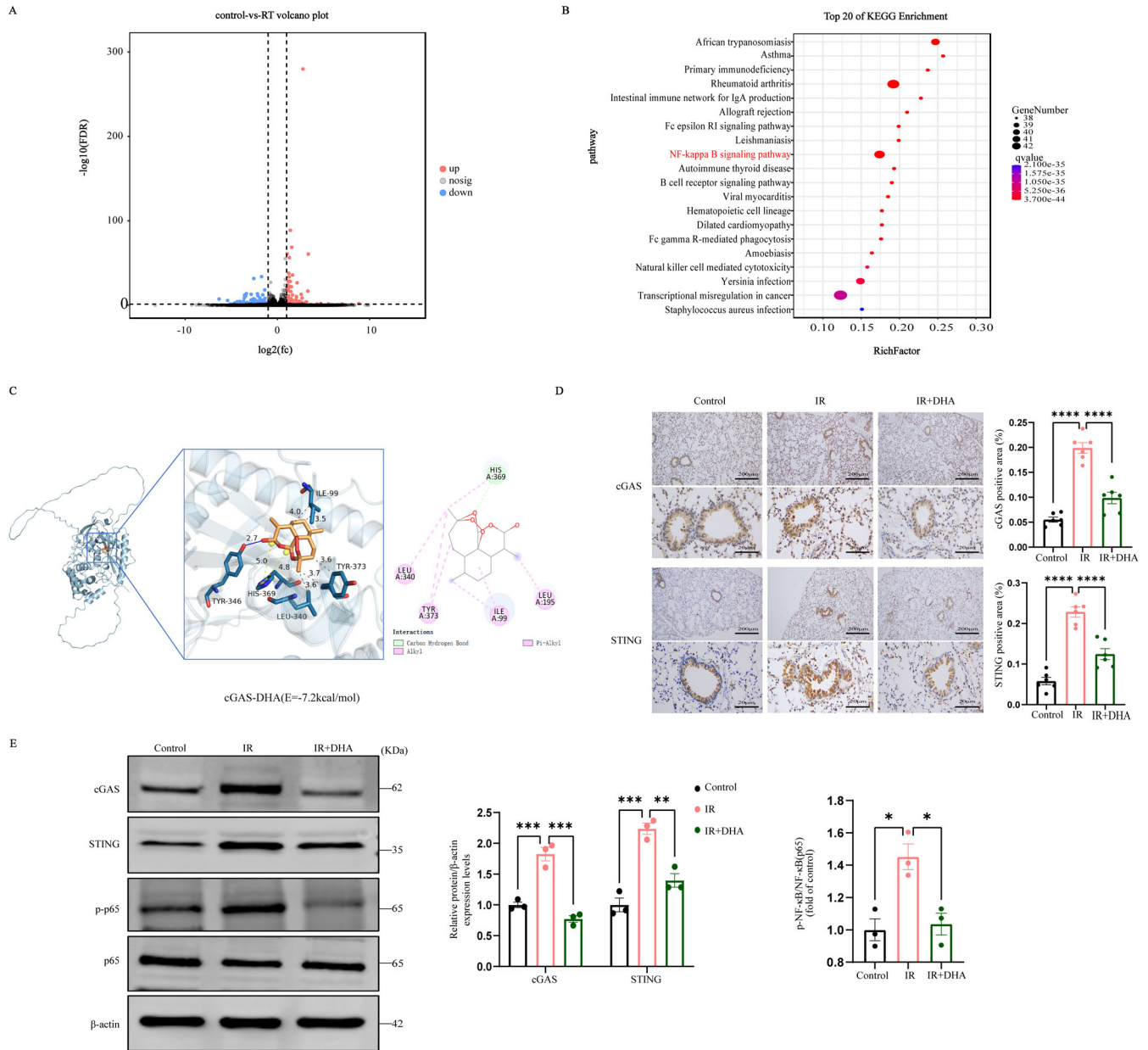
FIGURE 3 | DHA inhibited the expression of cGAS/STING/NF-κB signaling pathway in lung tissue. (A) Transcriptome analysis shown that there were significant changes in gene expression between the control group and the IR group. (B) Dotplot shown KEGG representative top20 pathway entries enriched in mouse lung tissue. (C) The affinity between DHA and cGAS was assayed through molecular docking; The affinity of the H-bond (TYR-346, HIS-369) was −7.2 kcal/mol. (D) Representative cGAS and STING IHC staining and semi-quantitative analysis were performed in mouse lung tissues. The cGAS-positive area ratios and the STING-positive area ratios. scale: 200 μm (×100) and 20 μm (×400). (E) Western blot of cGAS, STING, NF-κB and p-NF-κB proteins. Corresponding quantification of various proteins, and β-actin as the loading control. DHA, dihydroartemisinin; IR, irradiation; RT, radiotherapy. *$p < 0.05$, **$p < 0.01$, ***$p < 0.001$, ****$p < 0.0001$.

NF-κB, p-NF-κB. The results shown that the protein expression levels of cGAS, STING, and p-NF-κB were significantly increased in the irradiation group compared to the control group (Figure 5A). DHA pretreatment can reverse the increase in proteins such as cGAS, STING, and p-NF-κB caused by irradiation (Figure 5A). Similarly, qPCR also confirmed this result (Figure 5B). This suggested that DHA can reverse IR-induced inflammation by inhibiting the cGAS/STING/NF-κB pathway in BEAS-2B cells.

3.5 | Downregulating cGAS further Enhances the Alleviating Effects of DHA on RILI

To investigate the regulatory mechanism of the cGAS/STING/NF-κB pathway in irradiation-induced inflammation, we transfected BEAS-2B cells with siRNA. The results of qPCR and WB shown that cGAS was significantly knocked down after siRNA transfection, with the knockdown at the 1266 site being the most pronounced (Figure 6A,B). Subsequently, the
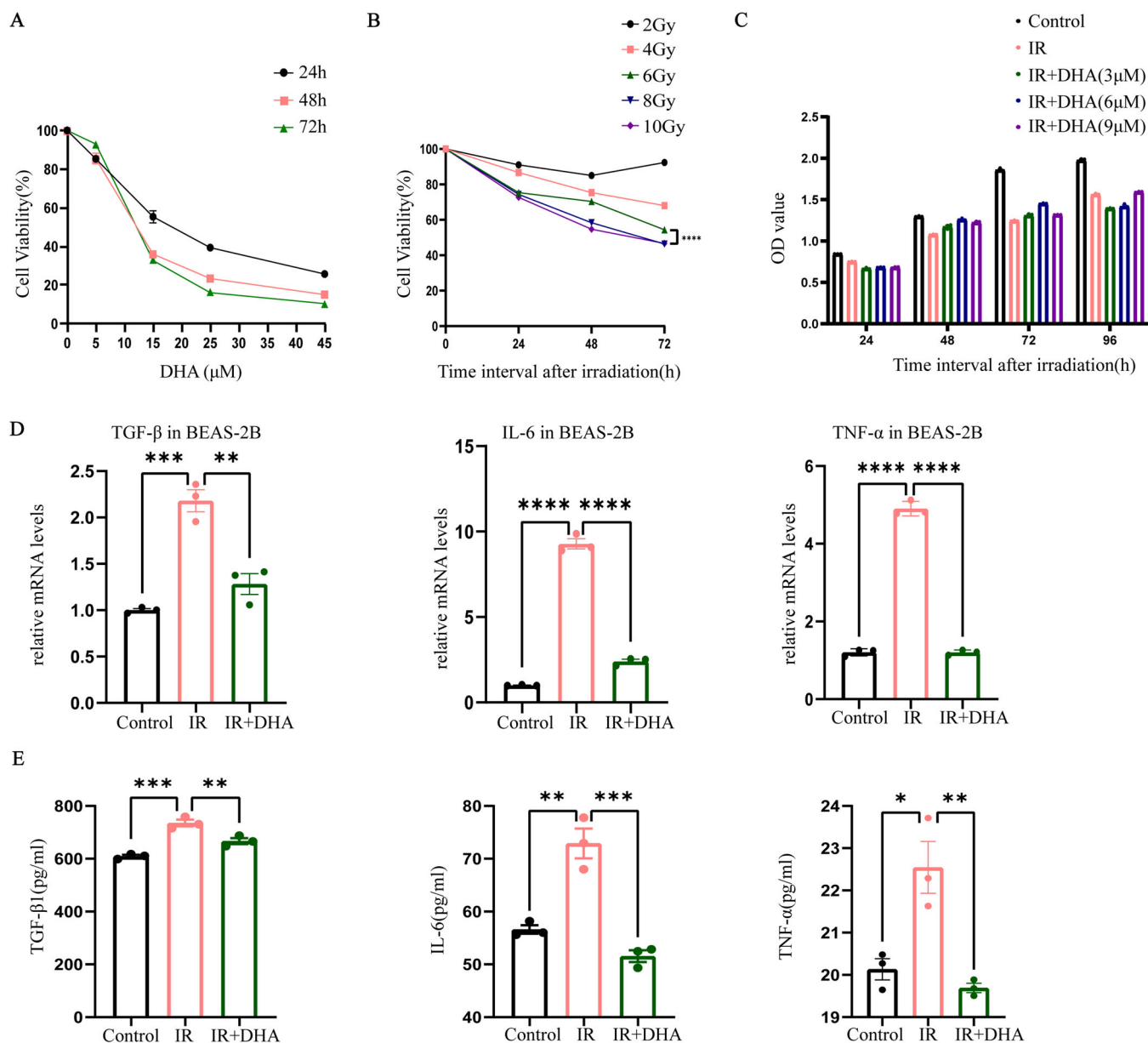
FIGURE 4 | DHA can reduce the damage of BEAS-2B cells. (A) The cell viability of BEAS-2B cells at different time points (24,48,72 h) at 0, 5, 15, 25, and 45 μM drug concentrations was detected by CCK-8 assay. (B) The cell viability of BEAS-2B cells at different time points after irradiation with 0, 2, 4, 6, 8, and 10 Gy was detected by CCK-8. (C) OD values of BEAS-2B cells at different drug concentrations and different time points after 8 Gy irradiation were measured by CCK-8. (D) Relative mRNA expression of TGF-β, IL-6 and TNF-α in BEAS-2B cells after irradiation. (E) The levels of TGF-β, IL-6 and TNF-α in the culture medium of BEAS-2B cells were detected by ELISA. CCK-8, Cell Counting Kit-8; DHA, dihydroartemisinin; IL-6, interleukin-6; TGF-β, transforming growth factor-β; TNF-α, tumor necrosis factorα; IR, irradiation. *$p < 0.05$, **$p < 0.01$, ***$p < 0.001$, ****$p < 0.0001$.

experiments were divided into irradiation group, irradiation-si-cGAS group, irradiation+DHA group and irradiation +DHA-si-cGAS group. The results of CCK8 assay shown that the cell viability of the other three groups was significantly increased compared with the irradiation group (Figure 6C), suggesting that knockdown of cGAS may play a protective role in cells. In addition, compared with the exposure to 8 Gy irradiation alone, the protein expressions of cGAS, STING, and p-NF-κB in the other groups decreased significantly. Compared with the irradiation-si-cGAS group, the protein expressions of cGAS, STING and p-NF-κB in the irradiation +DHA-si-cGAS group

were significantly decreased (Figure 6D). Further qPCR experiments also came to the same conclusion (Figure 6E). At the same time, we used an ELISA kit to detect the levels of TGF-β, IL-6, and TNF-α in the supernatant of BEAS-2B cells, and the results shown that the levels of TGF-β, IL-6, and TNF-α in the irradiation-si-cGAS group were significantly reduced compared with the irradiation group (Figure 6F). And the levels of TGF-β, IL-6 in the irradiation + DHA-si-cGAS group were significantly reduced compared with the irradiation + DHA group (Figure 6F). These results shown that si-cGAS down-regulated the effect of DHA in alleviating radiation lung injury.
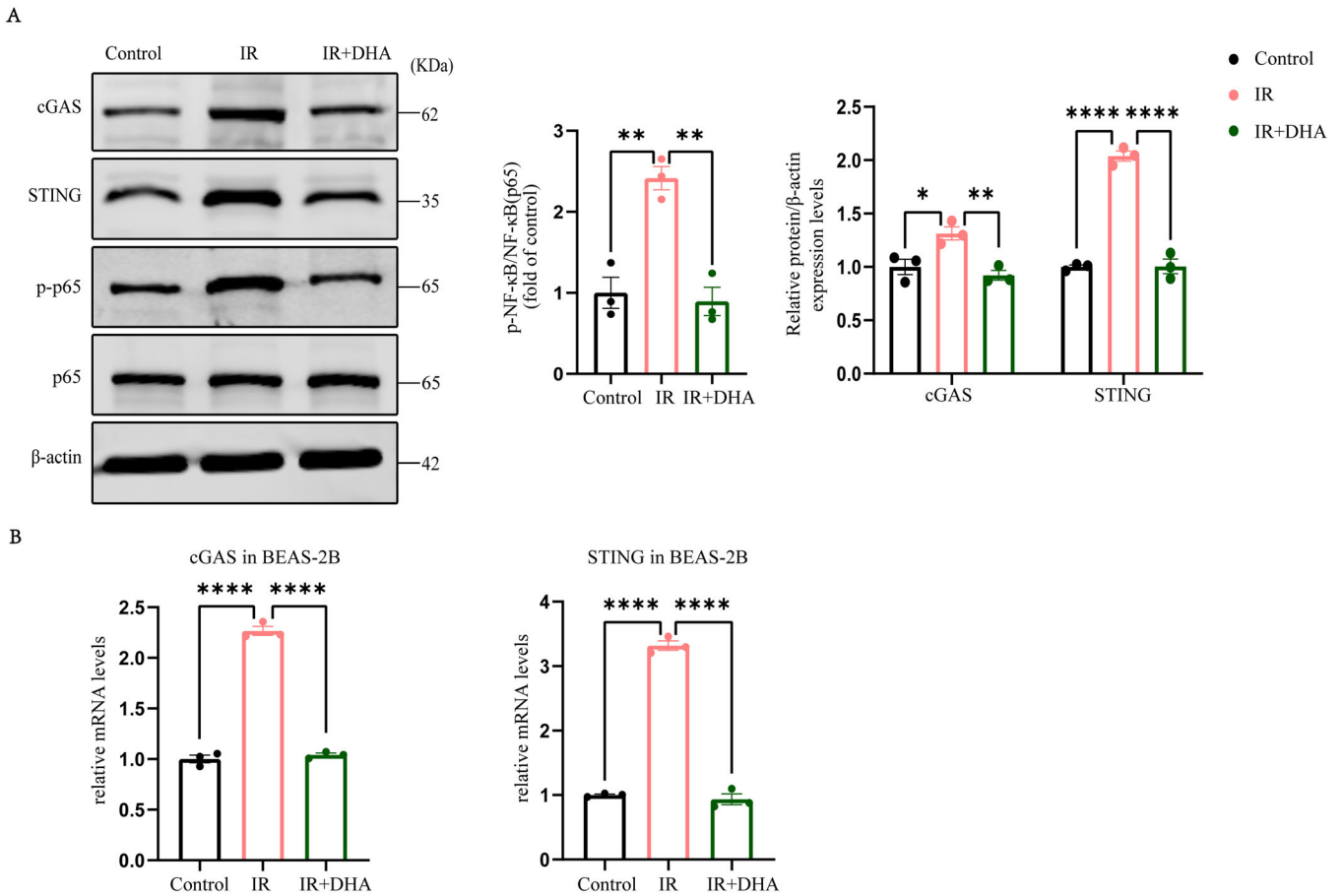
FIGURE 5 | DHA inhibited the expression of cGAS/STING/NF-κB signaling pathway in BEAS-2B cells. (A) Western blot of cGAS, STING, NF-κB and p-NF-κB proteins. Corresponding quantification of various proteins, and β-actin as the loading control. (B) Relative mRNA expression of cGAS and STING in BEAS-2B cells after irradiation. DHA, dihydroartemisinin; IR, irradiation. $*p < 0.05$, $**p < 0.01$, $***p < 0.001$, $****p < 0.0001$.

4 | Discussion

Respiratory failure or even death may result from untreated or postponed Grade IV lung injury following RILI (Käsmann et al. 2020). The degenerative alterations in the alveolar epithelium may be partially blocked or reversed if pharmacological treatments are given soon after irradiation (OASULLIVAN and Levin 2003). There are currently no viable treatment medications for RILI. In addition, RILI is now a challenging obstacle to the efficacy of thoracic RT, and its unique molecular mechanisms are largely unclear. In this study, we constructed a mouse model of RILI and an In Vitro cell model to discover the mechanism by which DHA mitigates RILI through the cGAS/STING/NF-κB pathway.

DHA is a well-known medication that effectively combats malaria. Interestingly, according to current research, DHA may lessen lung damage by decreasing fibrosis and inflammation in the lungs (Yang et al. 2018; You et al. 2022). However, the exact mode of action of DHA in RILI is unknown. In the RILI mice model, we used H&E and Masson staining to observe structural damage and collagen fibrillar deposition within the lungs. In addition, we also used IHC and ELISA assays to detect the expression of TGF-β, TNF-α, and IL-6. Treatment with DHA can improve these pathologies. Consistent with our previous experimental findings, the results demonstrated that DHA

administration was effective in improving the pathological alterations and reducing the expression of TGF-β, TNF-α, and IL-6 in the lung tissues (Ning et al. 2024).

It initially emerged that the cGAS-STING signaling pathway activates innate defense against microbial infections by monitoring harmful DNA. Strong evidence supported the idea that STING activation was an important variable in a number of inflammatory conditions, including non-alcoholic steatohepatitis (Luo et al. 2018; Yu et al. 2019), acute liver injury (Liu et al. 2022), sepsis-associated cardiac dysfunction (Li, Sun, et al. 2019; Li, Zhou, et al. 2019), and others. dsDNA is recognized by cGAS in a sequence-independent manner (Sun et al. 2013). Upon binding to DNA, its enzymatic function is activated, catalyzing the production of cGAMP, a unique hybrid-linked second messenger molecule that binds and activates STING (Ablasser et al. 2013). Activation of STING subsequently initiates a downstream transcriptional program majorly involving IFN, IRF3 and NF-κB to upregulate type I IFNs, pro-inflammatory cytokines and chemokines (Decout et al. 2021). According to reports, mitochondrial damage and the activation of the cGAS-STING pathway are intimately linked to renal fibrosis, which is caused by inflammation (Chung et al. 2019). For instance, in radiation-induced liver disease, dsDNA released from hepatocytes quickly triggered the cGAS-STING pathway in non-parenchymal cells, causing the
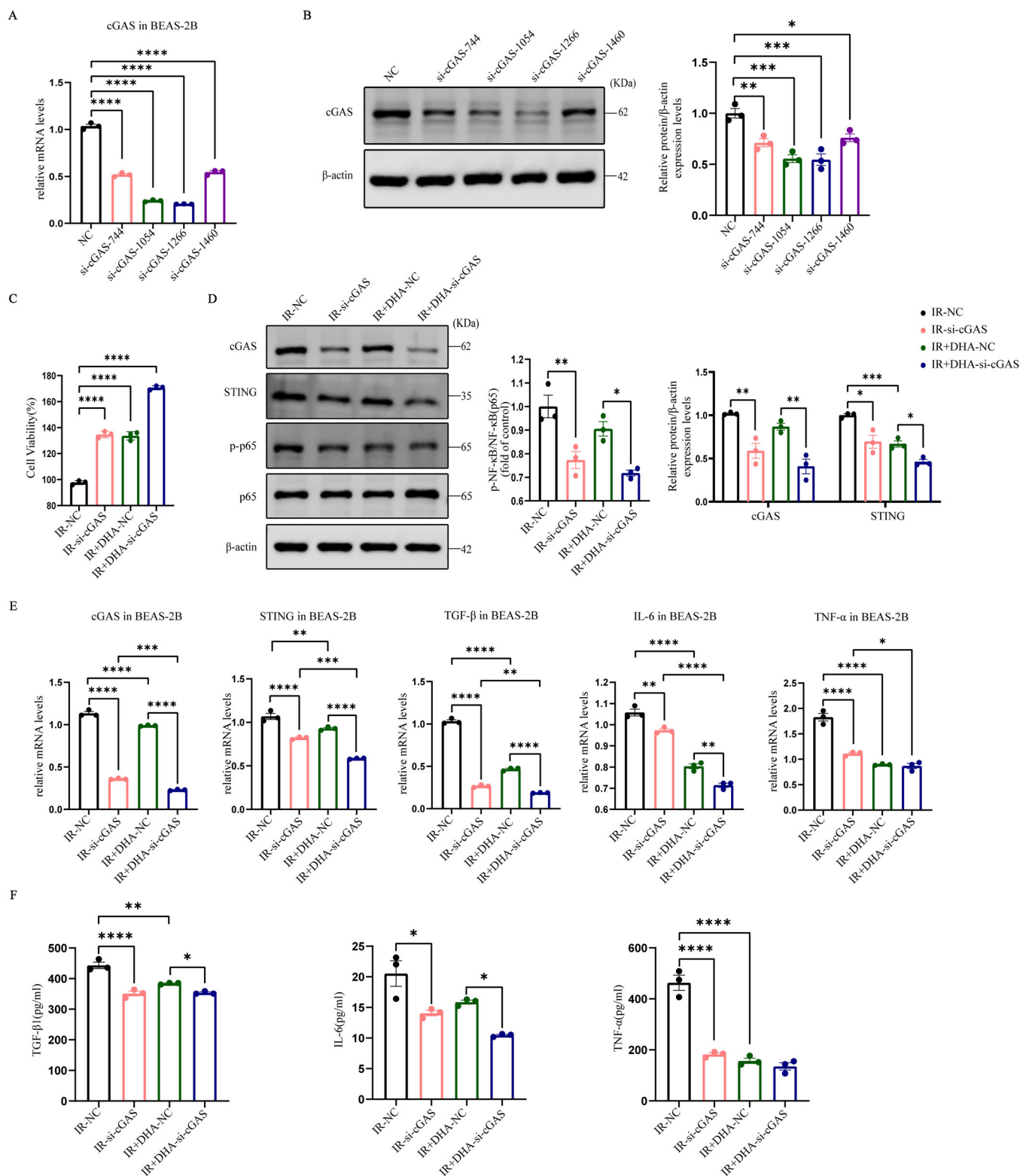
FIGURE 6 | Downregulating cGAS further enhances the alleviating effects of DHA on radiation-induced lung injury. (A) Relative mRNA expression and (B) Western blot of cGAS in BEAS-2B cells after siRNA transfection. (C) The cell viability of BEAS-2B cells transfected with siRNA after 8 Gy irradiation was detected by CCK-8. (D) Western blot of cGAS, STING, NF-κB and p-NF-κB proteins after siRNA transfection. Corresponding quantification of various proteins, and β-actin as the loading control. (E) Relative mRNA expression of cGAS, STING, TGF-β, IL-6 and TNF-α in BEAS-2B cells after siRNA transfection. (F) The levels of TGF-β, IL-6 and TNF-α in the culture medium of BEAS-2B cells after siRNA transfection were detected by ELISA. CCK-8, Cell Counting Kit-8; DHA, dihydroartemisinin; IR, irradiation; siRNA, small interfering RNA. *$p < 0.05$, **$p < 0.01$, ***$p < 0.001$, ****$p < 0.0001$.

TABLE 1 | List of the primer used in the present study.

Primer	Sequence
Homo cGAS forward	GGCCTGCGCATTCAAAACTG
Homo cGAS reverse	AGCCGCCATGTTTCTTCTTGG
Homo STING forward	TCTCGCAGGCACTGAACATC
Homo STING reverse	ACCCCGTAGCAGGTTGTTGT
Homo TGF-β forward	TGATGTCACCGGAGTTGTGC
Homo TGF-β reverse	CCGGTAGTGAACCCGTTGAT
Homo IL-6 forward	TTCGGTCCAGTTGCCTTCTC
Homo IL-6 reverse	CTGAGATGCCGTCGAGGATG
Homo TNF-α forward	CCTGCTGCACTTTGGAGTGAT
Homo TNF-α reverse	CAGCTTGAGGGGTTTGCTACAAC
Homo β-Actin forward	AGATCAAGATCATTGCTCCTCCTG
Homo β-Actin reverse	AGTCATAGTCCGCCTAGAAGCAT

synthesis and secretion of interferon-I and the simultaneous death of hepatocytes (Du et al. 2022). We performed transcriptome sequencing on the tissues of the control group and the radiation group, and found that STING was significantly different and enriched to the NF-KB pathway. Our experiments shown that the levels of cGAS/STING/NF-κB were significantly elevated after radiation, and downregulating cGAS can alleviated RILI, which were consistent with the results reported in the aforementioned literature.

DHA has many pharmacological effects on viral infection (Fröhlich et al. 2018), inflammation (Gao et al. 2020), and tumor proliferation (Malami et al. 2022). You et al. found that DHA can reduce lung inflammation and fibrosis in rats by inhibiting JAK2/STAT3 signaling (You et al. 2022). In addition, Gao et al. found that DHA can improve LPS-induced neuroinflammation by inhibiting the PI3K/AKT pathway (Gao et al. 2020). And Huang et al. found that DHA reduced lipopolysaccharide-induced acute lung injury in mice by inhibiting NF-κB signaling in a Nrf2-dependent manner (Huang et al. 2019). Additionally, Zhang et al. demonstrated that improving neuronal senescence following ischemic stroke involves blocking cGAS-STING activation by targeting the JAK2-STAT3 pathway (Zhang et al. 2023). Weng et al. discovered that in rheumatoid arthritis patients, macrophage extracellular traps enhanced tumor-like biologic characteristics of fibroblast-like synoviocytes via the cGAS-mediated PI3K/Akt signaling pathway (Weng et al. 2024). Therefore, it can be seen that the pathways related to DHA action are interrelated, which laid a theoretical foundation for our experiment. Our experimental results shown that down-regulation of cGAS can reduce the expression of downstream proteins STING and p-NF-κB, echoing the above reports.

There are some limitations to the current research. Firstly, in this study, rescue verification was performed on animals without drugs and we only used one cell line to verify in the experiment. Moreover, we did not further explore the detection of DNA damage by comet assay. In addition, cGAS is also linked to different types of death, and we did not explore a deeper mechanism of cell death. We will further investigate the specific regulatory mechanism of DHA regulation of cGAS/STING/NF-κB and thereby alleviate RILI.

In conclusion, this study shown that DHA alleviated RILI by inhibiting the cGAS/STING/NF-κB signaling pathway. Targeting cGAS-STING or inhibiting downstream NF-κB may represent promising therapeutic strategies for preventing RILI. DHA could be a suitable agent for the prevention and treatment of RILI, and its protective effects require further clinical trials.

Author Contributions

Cailan Wang: data curation, investigation, methodology, writing−original draft. **Xinyi Lin:** data curation, investigation, methodology. shichun guan: data curation, methodology. **Qiaoyuan Wu:** conceptualization, data curation, writing−review and editing. **Shixiong Liang:** conceptualization, project administration, supervision, writing−review and editing.

Ethics Statement

The animal procedures used in this study followed the standards for the Ethical Review of Animal Welfare in China (GB/T 35892-2018) and the research obtained approval from the Animal Experimentation Ethics Committee of Guangxi Medical University (No. 202205013).

Conflicts of Interest

The authors declare no conflicts of interest.

Data Availability Statement

Data generated or analyzed in this study are available from the authors upon reasonable request.

References

Ablasser, A., M. Goldeck, T. Cavlar, et al. 2013. "cGAS Produces a 2′-5′-Linked Cyclic Dinucleotide Second Messenger That Activates STING." *Nature* 498, no. 7454: 380–384. https://doi.org/10.1038/nature12306.

Abratt, R. P., G. W. Morgan, G. Silvestri, and P. Willcox. 2004. "Pulmonary Complications of Radiation Therapy." *Clinics in Chest Medicine* 25, no. 1: 167–177. https://doi.org/10.1016/S0272-5231(03)00126-6.

Azzam, E. I., J.-P. Jay-Gerin, and D. Pain. 2012. "Ionizing Radiation-Induced Metabolic Oxidative Stress and Prolonged Cell Injury." *Cancer Letters* 327, no. 1–2: 48–60. https://doi.org/10.1016/j.canlet.2011.12.012.

Barker, H. E., J. T. E. Paget, A. A. Khan, and K. J. Harrington. 2015. "The Tumour Microenvironment After Radiotherapy: Mechanisms of Resistance and Recurrence." *Nature Reviews Cancer* 15, no. 7: 409–425. https://doi.org/10.1038/nrc3958.

Benmerzoug, S., S. Rose, B. Bounab, et al. 2018. "STING-Dependent Sensing of Self-DNA Drives Silica-Induced Lung Inflammation." *Nature Communications* 9, no. 1: 5226. https://doi.org/10.1038/s41467-018-07425-1.

Carvalho, T. T., S. S. Mizokami, C. R. Ferraz, et al. 2019. "The Granulopoietic Cytokine Granulocyte Colony-Stimulating Factor (G-CSF) Induces Pain: Analgesia by Rutin." *Inflammopharmacology* 27, no. 6: 1285–1296. https://doi.org/10.1007/s10787-019-00591-8.

Chen, Q., L. Sun, and Z. J. Chen. 2016. "Regulation and Function of the cGAS–STING Pathway of Cytosolic DNA Sensing." *Nature Immunology* 17, no. 10: 1142–1149. https://doi.org/10.1038/ni.3558.

Chung, K. W., P. Dhillon, S. Huang, et al. 2019. "Mitochondrial Damage and Activation of the STING Pathway Lead to Renal Inflammation and Fibrosis." *Cell Metabolism* 30, no. 4: 784–799.e5. https://doi.org/10.1016/j.cmet.2019.08.003.

Curras-Alonso, S., J. Soulier, T. Defard, et al. 2023. "An Interactive Murine Single-Cell Atlas of the Lung Responses to Radiation Injury." *Nature Communications* 14, no. 1: 2445. https://doi.org/10.1038/s41467-023-38134-z.

Dai, X., X. Zhang, W. Chen, et al. 2021. "Dihydroartemisinin: A Potential Natural Anticancer Drug." *International Journal of Biological Sciences* 17, no. 2: 603–622. https://doi.org/10.7150/ijbs.50364.

Decout, A., J. D. Katz, S. Venkatraman, and A. Ablasser. 2021. "The cGAS–STING Pathway as a Therapeutic Target in Inflammatory Diseases." *Nature Reviews Immunology* 21, no. 9: 548–569. https://doi.org/10.1038/s41577-021-00524-z.

Du, S.-S., G.-W. Chen, P. Yang, et al. 2022. "Radiation Therapy Promotes Hepatocellular Carcinoma Immune Cloaking via PD-L1 Upregulation Induced by cGAS-STING Activation." *International Journal of Radiation Oncology*Biology*Physics* 112, no. 5: 1243–1255. https://doi.org/10.1016/j.ijrobp.2021.12.162.

Fröhlich, T., F. Hahn, L. Belmudes, et al. 2018. "Synthesis of Artemisinin-Derived Dimers, Trimers and Dendrimers: Investigation of Their Antimalarial and Antiviral Activities Including Putative Mechanisms of Action." *Chemistry (Weinheim an der Bergstrasse, Germany)* 24, no. 32: 8103–8113. https://doi.org/10.1002/chem.201800729.

Gao, Y., M. Cui, S. Zhong, et al. 2020. "Dihydroartemisinin Ameliorates LPS-Induced Neuroinflammation by Inhibiting the PI3K/AKT Pathway." *Metabolic Brain Disease* 35, no. 4: 661–672. https://doi.org/10.1007/s11011-020-00533-2.

Hanania, A. N., W. Mainwaring, Y. T. Ghebre, N. A. Hanania, and M. Ludwig. 2019. "Radiation-Induced Lung Injury." *Chest* 156, no. 1: 150–162. https://doi.org/10.1016/j.chest.2019.03.033.

Huang, X.-T., W. Liu, Y. Zhou, et al. 2019. "Dihydroartemisinin Attenuates Lipopolysaccharide-Induced Acute Lung Injury in Mice by Suppressing NF-κB Signaling in an Nrf2-dependent Manner." *International Journal of Molecular Medicine* 44, no. 6: 2213–2222. https://doi.org/10.3892/ijmm.2019.4387.

Käsmann, L., A. Dietrich, C. A. Staab-Weijnitz, et al. 2020. "Radiation-Induced Lung Toxicity—Cellular and Molecular Mechanisms of Pathogenesis, Management, and Literature Review." *Radiation Oncology* 15, no. 1: 214. https://doi.org/10.1186/s13014-020-01654-9.

Li, N., W. Sun, X. Zhou, et al. 2019. "Dihydroartemisinin Protects Against Dextran Sulfate Sodium-Induced Colitis in Mice Through Inhibiting the PI3K/AKT and NF-κB Signaling Pathways." *BioMed Research International* 2019: 1415809. https://doi.org/10.1155/2019/1415809.

Li, N., H. Zhou, H. Wu, et al. 2019. "STING-IRF3 Contributes to Lipopolysaccharide-Induced Cardiac Dysfunction, Inflammation, Apoptosis and Pyroptosis by Activating NLRP3." *Redox Biology* 24: 101215. https://doi.org/10.1016/j.redox.2019.101215.

Li, W., Y. Dong, Y. Tu, and Z. Lin. 2006. "Dihydroarteannuin Ameliorates Lupus Symptom of BXSB Mice by Inhibiting Production of TNF-Alpha and Blocking the Signaling Pathway NF-Kappa B Translocation." *International Immunopharmacology* 6, no. 8: 1243–1250. https://doi.org/10.1016/j.intimp.2006.03.004.

Liu, Z., M. Wang, X. Wang, et al. 2022. "XBP1 Deficiency Promotes Hepatocyte Pyroptosis by Impairing Mitophagy to Activate mtDNA-cGAS-STING Signaling in Macrophages During Acute Liver Injury." *Redox Biology* 52: 102305.

Luo, X., H. Li, L. Ma, et al. 2018. "Expression of STING is Increased in Liver Tissues From Patients With NAFLD and Promotes Macrophage-Mediated Hepatic Inflammation and Fibrosis in Mice." *Gastroenterology* 155, no. 6: 1971–1984.e4. https://doi.org/10.1053/j.gastro.2018.09.010.

Malami, I., A. M. Bunza, A. M. Alhassan, et al. 2022. "Dihydroartemisinin as a Potential Drug Candidate for Cancer Therapy: A Structural-Based Virtual Screening for Multitarget Profiling." *Journal of Biomolecular Structure & Dynamics* 40, no. 3: 1347–1362. https://doi.org/10.1080/07391102.2020.1824811.

Matute-Bello, G., G. Downey, B. B. Moore, et al. 2011. "An Official American Thoracic Society Workshop Report: Features and Measurements of Experimental Acute Lung Injury in Animals." *American Journal of Respiratory Cell and Molecular Biology* 44, no. 5: 725–738. https://doi.org/10.1165/rcmb.2009-0210ST.

Ning, X., W. Zhao, Q. Wu, C. Wang, and S. Liang. 2024. "Therapeutic Potential of Dihydroartemisinin In Mitigating Radiation-Induced Lung Injury: Inhibition of Ferroptosis Through Nrf2/HO-1 Pathways in Mice." *Immunity, Inflammation and Disease* 12, no. 2: e1175. https://doi.org/10.1002/iid3.1175.

Oasullivan, B., and W. Levin. 2003. "Late Radiation-Related Fibrosis: Pathogenesis, Manifestations, and Current Management." *Seminars in Radiation Oncology* 13, no. 3: 274–289. https://doi.org/10.1016/S1053-4296(03)00037-7.

Ryter, S. W., H. P. Kim, A. Hoetzel, et al. 2007. "Mechanisms of Cell Death in Oxidative Stress." *Antioxidants & Redox Signaling* 9, no. 1: 49–89. https://doi.org/10.1089/ars.2007.9.49.

Sun, L., J. Wu, F. Du, X. Chen, and Z. J. Chen. 2013. "Cyclic GMP-AMP Synthase Is a Cytosolic DNA Sensor That Activates the Type I Interferon Pathway." *Science* 339, no. 6121: 786–791. https://doi.org/10.1126/science.1232458.

Wang, L., W. Zhao, X. Ning, C. Wang, and S. Liang. 2023. "Effect of X-Ray Irradiation Combined With PD-1 Inhibitor Treatment on Lung Tissue Injury in Mice." *International Immunopharmacology* 123: 110775. https://doi.org/10.1016/j.intimp.2023.110775.

Weng, W., Y. Liu, Z. Hu, et al. 2024. "Macrophage Extracellular Traps Promote Tumor-Like Biologic Behaviors of Fibroblast-Like Synoviocytes through cGAS-Mediated PI3K/Akt Signaling Pathway in Patients With Rheumatoid Arthritis." *Journal of Leukocyte Biology* 115, no. 1: 116–129. https://doi.org/10.1093/jleuko/qiad102.

Xu, H., Y. He, X. Yang, et al. 2007. "Anti-Malarial Agent Artesunate Inhibits TNF- -Induced Production of Proinflammatory Cytokines via Inhibition of NF-B and PI3 Kinase/AKT Signal Pathway in Human Rheumatoid Arthritis Fibroblast-Like Synoviocytes." *Rheumatology* 46, no. 6: 920–926. https://doi.org/10.1093/rheumatology/kem014.

Yang, D., J. Qiu, H.-H. Zhou, et al. 2018. "Dihydroartemisinin Alleviates Oxidative Stress in Bleomycin-Induced Pulmonary Fibrosis." *Life Sciences* 205: 176–183. https://doi.org/10.1016/j.lfs.2018.05.022.

You, X., X. Jiang, C. Zhang, et al. 2022. "Dihydroartemisinin Attenuates Pulmonary Inflammation and Fibrosis in Rats by Suppressing JAK2/STAT3 Signaling." *Aging* 14, no. 3: 1110–1127. https://doi.org/10.18632/aging.203874.

Yu, Y., Y. Liu, W. An, J. Song, Y. Zhang, and X. Zhao. 2019. "STING-Mediated Inflammation In Kupffer Cells Contributes to Progression of Nonalcoholic Steatohepatitis." *Journal of Clinical Investigation* 129, no. 2: 546–555. https://doi.org/10.1172/JCI121842.

Zhang, W., M. Xu, F. Chen, et al. 2023. "Targeting the JAK2-STAT3 Pathway to inhibit cGAS-STING Activation Improves Neuronal Senescence After Ischemic Stroke." *Experimental Neurology* 368: 114474. https://doi.org/10.1016/j.expneurol.2023.114474.

Zhong, S., Q. Zhou, J. Yang, et al. 2024. "Relationship Between the cGAS−STING and NF-κB Pathways-Role in Neurotoxicity." *Biomedicine & Pharmacotherapy = Biomedecine & Pharmacotherapie* 175: 116698. https://doi.org/10.1016/j.biopha.2024.116698.

Supporting Information

Additional supporting information can be found online in the Supporting Information section.